NOVEL MEASUREMENT METHOD FOR LOCAL WALL SHEAR STRESS IN HIGH REYNOLDS NUMBER FLOWS BY UTILIZING FRESNEL'S BIPRISM

Katsuaki Shirai, Keisuke Tsuru and Shinnosuke Obi
Department of Mechanical Engineering, Keio University
3-14-1 Hiyoshi, Yokohama, 223-8522, Japan
td04617@educ.cc.keio.ac.jp (Shirai)

ABSTRACT

A novel measurement method for local wall shear stress is proposed for the measurement in a high Reynolds number flow. The method utilizes the light interference created by a Fresnel's biprism. The biprism method can be applied to the flow where a conventional slit-type method can not be applied. In this paper, we propose two types of optical configurations for the biprism sensor. The principle is investigated with respect to the light interference and the measurement volume. The interference patterns created by the two types of configurations are calculated by electromagnetic theory. The results show the interference pattern created by the proposed configurations is not suitable for the local wall shear stress measurement. Considerations are required before the method is applied to the measurement in a flow.

INTRODUCTION

Wall shear stress is one of the important parameters for understanding the wall bounded flows. It is related to skin friction, separation and scaling of flow near the wall. In turbulent flows, the fluctuating local wall shear stress indicates the process related to the unsteady momentum transfer to the wall while the time-averaged mean wall shear stress indicates the global state of the flow over a surface (Haritonidis, 1989). In order to elucidate the near-wall structure of turbulent flows, it is necessary to obtain the information of fluctuating wall shear stress with a sufficient temporal and spatial resolution.

Measurement method for the fluctuating wall shear stress is restricted while there have been many measurement methods for wall shear stress. Sensors based on the micro-electro-mechanical-systems can be fabricated aiming at the measurement with a high temporal and spatial resolution (Padmanabhan et al., 1996, Löfdahl and Gad-el-Hak, 1999, Chandrasekaran et al., 2001). However they need calibration which affects the accuracy of the measurement (Haritonidis, 1989). Another method to measure the fluctuating wall shear stress is to measure the instantaneous velocity gradient near the wall using a hot-wire anemometer or a laser Doppler anemometer (Alfredsson et al., 1988, Durst et al., 1995). The method is affected by the uncertainty of the location of measurement volume with respect to the wall and the steep velocity gradient within the measurement volume while some solutions have been proposed (Durst et al., 1998, Czarske et al., 2002).

Naqwi and Reynolds (1984, 1991) proposed an optical measurement method for local wall shear stress by extending the laser Doppler technique. They utilized two optical slits formed on the wall to create a fan-like interference pattern to measure the wall shear stress. Using the slits method, several measurements have been conducted in turbulent flows. Naqwi and Renyolds (1991), Millerd et al. (1996) and Obi et al. (1996) obtained good agreement with the result of direct numerical simulations of low Reynolds number turbulent flow. On the other hand, Sun (1987) and Sun and Qe (1991) utilize Fresnel's biprism to create fan-like interference pattern. They confirmed the capability of the method in a laminar boundary layer of a flow.

Though the frequency shift technique can not be used, biprism configuration is capable of applying the method to high Reynolds number flows where a sensor of slit configuration can not be applied. In contrast, the slit configuration has an advantage of using frequency shift to detect the flow direction. The optical alignment for the biprism configuration is considered not to be difficult compared with the slit configuration.

In this study, the feasibility of the methods using Fresnel's biprism is investigated. We propose two types of configurations aiming at the application to high Reynolds number flows. The principle and the measurement volume of the method is introduced by electromagnetic theory. Then the interference patterns created by the two types of configurations are calculated as the intensity of electric field. The spacings of the interference fringes are extracted and the possibility of applying the sensor to a high Reynolds number flow is discussed.

PRINCIPLE

Interference by Biprism

The interference created by a biprism is explained by electromagnetic theory. Fresnel's biprism is one of the devices to create interference pattern like Young's interference (Born and Wolf, 1999, Hecht, 2002). The prism consists of two equal prisms of small refracting angle joined together at their bases (Fig. 1).

The axis x and y is taken to the spanwise direction of the prism and the incident direction of light. We treat the

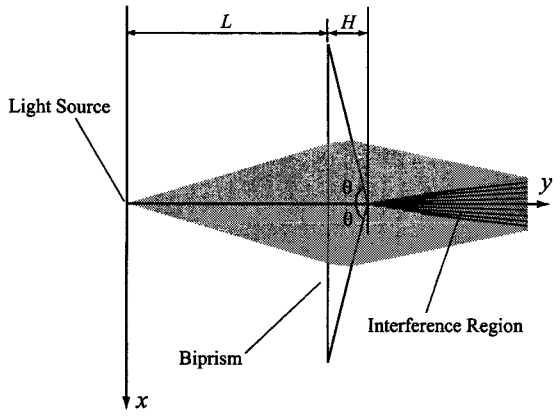

Figure 1: Axes and the geometry of the biprism

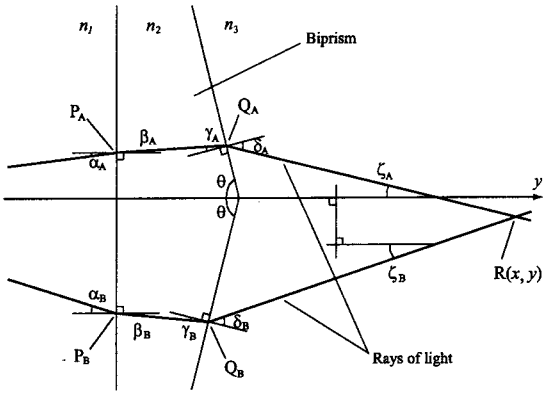

Figure 2: Rays of light propagating in the biprism

system two-dimensionally in the following if the prism is uniform in the depth direction.

A divergent light is incident into a biprism from flat side of the prism as shown in Fig. 1. The biprism has half the vertex angle of θ. The incident light is divided into two components when they reach at the second surface of the prism. The divided lights interfere after emanating from the prism.

The interference pattern created by a biprism is considered by the superposition of electric field based on electromagnetic theory. The interference is created by the upper side ($x < 0$) and the lower side ($x > 0$) of incident light (Fig. 2). If the incident light is polarized perpendicular to the x-y plane, the electric fields are described by

$$E_{1A} = E_1 \exp\{j[\omega t - k_1(-x\sin\alpha_A + y\cos\alpha_A) + \phi_{1A}]\}, \quad (1)$$

$$E_{1B} = E_1 \exp\{j[\omega t - k_1(\ x\sin\alpha_B + y\cos\alpha_B) + \phi_{1B}]\}, \quad (2)$$

where E and ϕ denote the amplitude and the phase of the electric fields. ω, t, j and α are used for the angular frequency of light, time, the imaginary unit and the incident angle at the first surface, respectively. The subscript A, B, 1 denote the quantity related to the upper side ($x < 0$), the lower side ($x > 0$) and the first medium, respectively. k_1 is the wavenumber in the first medium as defined by

$$k_1 = \frac{2\pi n_1}{\lambda}, \quad (3)$$

where λ and n are the wavelength of the light and the refractive index, respectively. Each of the incident light refracts at the first surface of incidence at x=L. The boundary conditions of electric fields at the first surface give the relations

$$n_1 \sin\alpha_A = n_2 \sin\beta_A, \quad (4)$$

$$n_1 \sin\alpha_B = n_2 \sin\beta_B, \quad (5)$$

where the subscript 2 indicates the quantity related to the second medium (biprism) and β is the refraction angle at the first surface. The boundary condition of the phase at the intersection point P of the first surface follows

$$\phi_{2A}\big|_{P_A} = \phi_{1A}\big|_{P_A}, \quad (6)$$

$$\phi_{2B}\big|_{P_B} = \phi_{1B}\big|_{P_B}, \quad (7)$$

which indicate the continuity of phase at the first surface. Then the electric fields in the second medium are written by

$$E_{2A} = E_2 \exp\{j[\omega t - k_2(-x\sin\beta_A + y\cos\beta_A) + \phi_{2A}]\}, \quad (8)$$

$$E_{2B} = E_2 \exp\{j[\omega t - k_2(\ x\sin\beta_B + y\cos\beta_B) + \phi_{1B}]\}, \quad (9)$$

where k_2 is the wavenumber in the second medium as defined by

$$k_2 = \frac{2\pi n_2}{\lambda}. \quad (10)$$

The boundary conditions at the second surface give the relation for refraction

$$n_2 \sin\gamma_A = n_3 \sin\delta_A, \quad (11)$$

$$n_2 \sin\gamma_B = n_3 \sin\delta_B, \quad (12)$$

where γ and δ denote the incident angle and the refraction angle at the second surface. The subscript 3 is used for the quantity related to the third medium. β and γ have the relationships as

$$\beta_A + \gamma_A + \theta = \frac{\pi}{2}, \quad (13)$$

$$\beta_B + \gamma_B + \theta = \frac{\pi}{2}. \quad (14)$$

The boundary condition of the phase at the intersection point Q of the second surface follows

$$\phi_{3A}\big|_{Q_A} = \phi_{2A}\big|_{Q_A}, \quad (15)$$

$$\phi_{3B}\big|_{Q_B} = \phi_{2B}\big|_{Q_B}, \quad (16)$$

which indicate the continuity of phase at the second surface. The electric fields of the refracted lights in the third medium are described as

$$E_{3A} = E_3 \exp\{j[\omega t - k_3(\ x\sin\zeta_A + y\cos\zeta_A) + \phi_{3A}]\}, \quad (17)$$

$$E_{3B} = E_3 \exp\{j[\omega t - k_3(-x\sin\zeta_B + y\cos\zeta_B) + \phi_{3B}]\}, \quad (18)$$

where ζ is the angle with respect to the y-axis as shown in Fig. 2. k_3 is the wavenumber in the third medium as defined by

$$k_3 = \frac{2\pi n_3}{\lambda}. \quad (19)$$

The angles δ and ζ have the relationships as

$$\delta_A - \zeta_A + \theta = \frac{\pi}{2}, \quad (20)$$

$$\delta_B - \zeta_B + \theta = \frac{\pi}{2}. \quad (21)$$

The lights refracted at the second surface interfere and the energy density of the superposed electric field in the interference region is given by

$$\psi = \varepsilon_3 (E_{3A} + E_{3B})^2 = 4\varepsilon_3 {E_3}^2 \cos^2\chi_a \cos^2\chi_b, \quad (22)$$

where ε_3 is the permittivity of the third medium. The first cosine term in the above equation denotes the amplitude and the second cosine term oscillates with time,

$$\chi_a = -k_3 \frac{(x\sin\zeta_A + y\cos\zeta_A) - (x\sin\zeta_B + y\cos\zeta_B)}{2} + \frac{\phi_{3A} - \phi_{3B}}{2}, \quad (23)$$

$$\chi_b = \omega t - k_3 \frac{(-x\sin\zeta_A + y\cos\zeta_A) + (-x\sin\zeta_B + y\cos\zeta_B)}{2} + \frac{\phi_{3A} + \phi_{3B}}{2}. \quad (24)$$

Time-averaging the energy density over one period yields the intensity (irradiance) of the electromagnetic field (Hecht, 2002, Albrecht et al., 2002),

$$I = c\varepsilon_3 {E_3}^2 \left[1 + \cos 2\chi_a\right], \quad (25)$$

where c is the speed of light in the third medium. The interference pattern is created by bright and dark fringes. The bright fringes are created when the cosine function takes local maximum value in the Eq.(25),

$$\chi_a = m\pi, \ (m = 0, \pm 1, \pm 2, \cdots). \quad (26)$$

We treat two types of sensors in this paper as depicted in Fig. 3. Type I sensor utilizes an ordinary biprism and type II sensor utilize an ordinary prism with additional two sub-prisms so that the sensor head can be mounted flush to the wall. Type I sensor seems to affect the flow by its convex sharp angle of vertex at a glance. But the vertex angle is not considered to seriously affect the flow if a small biprism is used. The electric field of the type II sensor is calculated by a straight forward manner as the above procedures except for the additional refraction caused by the sub-prisms. If the refractive index of the sub-prisms are matched to that of the working fluid, the electric field of type II sensor is almost identical to that of the type I sensor.

Doppler Frequency and Wall Shear Stress

A fringe model is used to consider the Doppler frequency. We set flow axis X and Y as mean flow direction and the wall-normal direction, respectively. The Doppler frequency f_d is described by

$$f_d = \frac{U}{d}, \quad (27)$$

where U and d denote the velocity of tracer particle in the X-direction and the spacing of the interference fringes in the X-direction created by the biprism, respectively (Fig. 3). When the measurement volume is within the viscous sublayer, the mean velocity of a tracer particle becomes a linear function of the height from the wall,

$$U = \frac{\tau_w}{\mu} Y, \quad (28)$$

where τ_w is the wall shear stress and μ is the viscosity of fluid. If the fringe spacing becomes a linear function of Y,

$$d = GY, \quad (29)$$

the wall shear stress is directly determined by the Doppler frequency irrespective to the height of a tracer particle passing through the measurement volume,

$$\tau_w = \mu G f_d. \quad (30)$$

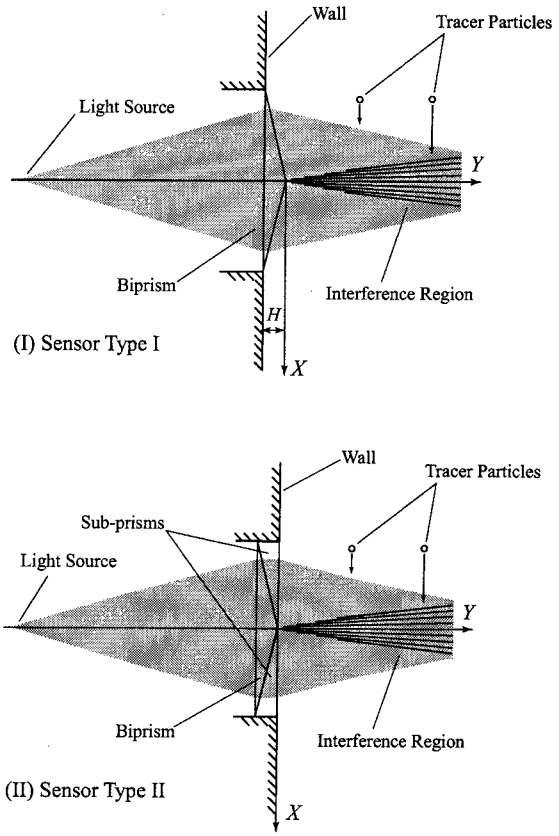

Figure 3: Two types of configurations of biprism sensor

Measurement Volume

The measurement volume is defined by the two factors, i.e., the interference region and the region observed by the receiving optics. As the latter depends on the optics used in each sensor system, we only consider the former in the paper.

For simplicity, the interference pattern is considered only for type I sensor here. The interference region is formed by the two refracted lights and the edge of the region can be found by considering the limit of incident angle. As setting α close to be zero, β becomes close to zero (Eqs.(4) and (5)) and γ becomes close to $(\frac{\pi}{2} - \theta)$ (Eqs.(20) and (21)). Then the Eqs.(11) and (12) give the limiting path of lights (Fig. 4). Here it can be noticed that the interference pattern can not be created if the total reflection occurs at the second surface. It is important to set the interference region as close to the wall as possible in order to conduct a measurement in a high Reynolds number flow. Because the thickness of the viscous sublayer becomes thinner as the Reynolds number increases while the principle is only valid in the viscous sublayer. In order to avoid the total reflection at the second surface, the following condition must be satisfied for the biprism,

$$\theta \geq \cos^{-1}\left(\frac{n_3}{n_2}\right). \quad (31)$$

If the Eq.(31) is not met, the interference pattern can not be created. The equality in the Eq.(31) gives critical value of θ. Typical critical value of θ becomes $\theta_{critical} = 48^\circ$ when the biprism is made of BK7 (n_2=1.51) and the fluid is air (n_3=1.0).

The interference occurs just from the vertex of the biprism (Y=0 in Fig. 3). But the bound of the interference region is restricted by the refraction at the second surface.

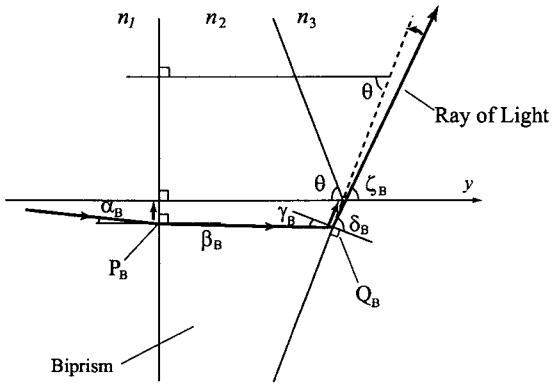

Figure 4: Ray of light in the biprism near the condition of total reflection

The bound is determined by considering the limit of the incident angle similar to the above. The interference region becomes

$$Y \geq \frac{1}{\tan\zeta\big|_{\alpha\to 0}} |X| . \qquad (32)$$

The interference region of the type II sensor can also be obtained with a similar way by setting the incident angle close to zero.

CALCULATION PROCEDURE

The calculation procedure for the interference pattern is described. We calculate the distribution of the intensity of the electric field by tracing the ray of light emanating from the source.

At first, a point (X, Y) to be calculated the intensity is set and the diverging angle α is changed moderately. Once α is selected, the path of light is determined by the boundary conditions of refractions at the prism surfaces explained in the principle. If the light passes through the point considered, α for the point is determined. Otherwise, another α is the next candidate for the point. The appropriate α for a point is determined by choosing the most likely α with which light passes through the point. By repeating the above procedure for the entire points of calculation, all the α for the points is determined for the light from the upper half and lower half of the biprism. Then the electric field of each point is calculated with the determined α and hence the intensity of the electric field is calculated by the equations described in the principle. The calculation is conducted for the region of $X>0$ and $Y>0$ as the optical geometry is symmetrical with respect to the Y-axis. In the present work, the decay of the amplitude of light is not considered though the intensity of light decays inversely as the distance from the light source.

RESULTS

Interference Pattern

The interference patterns created by the two optical configurations of biprism sensors were investigated. The intensity of the electric fields for the incident light was calculated in the region where the refracted lights exist. The refractive index of optical glass ranges from 1.4 to 1.9 (Sumita Optical Glass Inc., 2002). The combination of quantities used for the calculation is listed in Table 1. The first and the last

Table 1: Refractive indices used for the calculation

	Type I	Type II
n_1	1.00	1.00
n_2	1.51	1.89
n_3	1.00	1.43
n_4	-	1.00

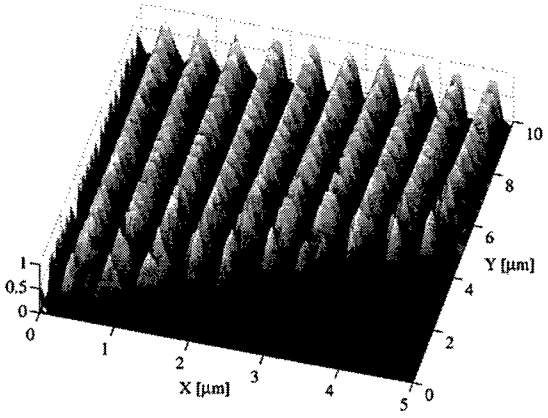

Figure 5: The distribution of the light intensity for the type I sensor (The intensity increases form black to white.)

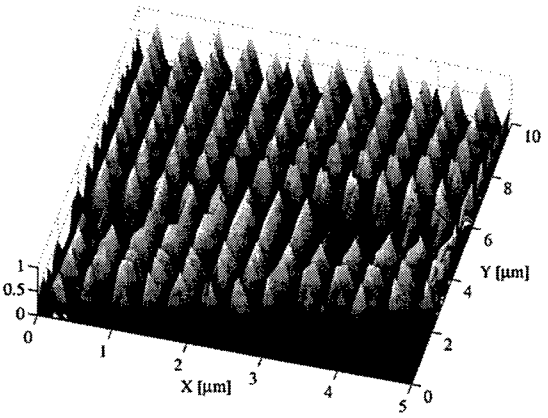

Figure 6: The distribution of the light intensity for the type II sensor (The intensity increases form black to white.)

medium for both types of sensors were air which is same for the working fluid considered. The wavelength of the incident light was λ=670 nm. Half the vertex angle of the biprism θ was chosen so that it becomes critical angle for the Eq.(31). L=10 mm and H=5 mm were used for the distance from the light source to the the first surface and the thickness of the biprism.

The interference pattern calculated for the two configurations are shown in Fig. 5 and Fig. 6. The intensities were normalized so that the maximum intensity becomes unity. Bright and dark patterns diverging into Y-direction can be seen in the interference pattern. The white portion in the figures indicates the higher intensity of electric field that corresponds to the bright region of the interference and the black portion indicates the opposite which corresponds to

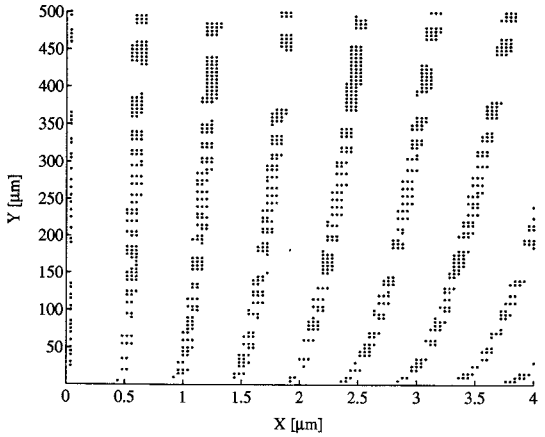

Figure 7: The fringe pattern created by the type I sensor (The dots show the bright points of the interference pattern.)

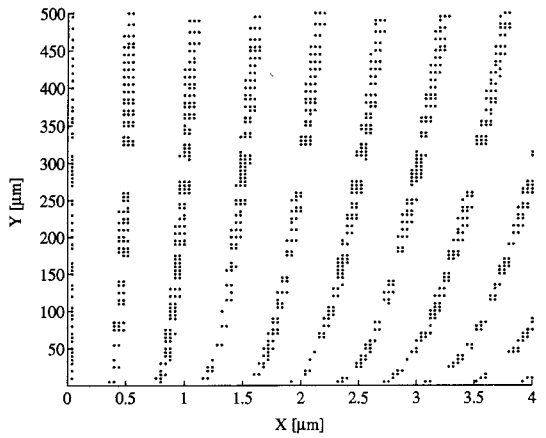

Figure 8: The fringe pattern created by the type II sensor (The dots show the bright points of the interference pattern.)

the dark region of the interference.

The interferences begin to occur just above from the wall ($Y = 0$) as expected for both types of sensors. However the fringes are not fan-like shape which is suitable for the local wall shear stress measurement. The interference pattern of the type I sensor (Fig. 5) is nearly parallel but is slightly diverges in the Y-direction. The interference pattern of the type II sensor (Fig. 6) is similar to that of the type I sensor but the density of the pattern is higher than that of the type I sensor in the same size of the area. The lower bound of the measurement volume of the type II sensor is lower than that of the type I sensor because of the additional refraction by the sub-prisms of the type II sensor.

Fringe Spacing

In order to obtain the spacings of the interference fringes respect to the height from the wall, the bright lines were extracted from the interference pattern. The bright lines are plotted as groups of bright points in Fig. 7 and Fig. 8. The points whose intensity of electric field are larger than 90 % of the maximum intensity were extracted as the bright points. While it was expected that the interference patterns become fan-like shapes and the fringe spacings linearly increase with increasing Y from the wall, the spacings have offsets at the wall. The interference pattern created by the present configurations of biprism sensor is not preferable to the measurement of local wall shear stress.

DISCUSSION

The interferences begin to occur just from the wall surface as expected for both types of the configurations. However, the interference patterns are not preferable to the local wall shear stress measurement because the fringe spacings have offsets at the wall surface for both types of sensors. The reason for the offset is found by considering the virtual sources of refracted lights. Each of the lights refracted at the second (third for the type II sensor) surface of the biprism has a virtual source before incident into the biprism as shown in Fig. 9. The interference created by the biprism is equivalent to the interference pattern created by the diffracted lights from two slits located at the virtual sources. The interference pattern created by two slits becomes fan-like shape, which diverges from the plane where the slits are located. Therefore the offset at the wall can be reduced by

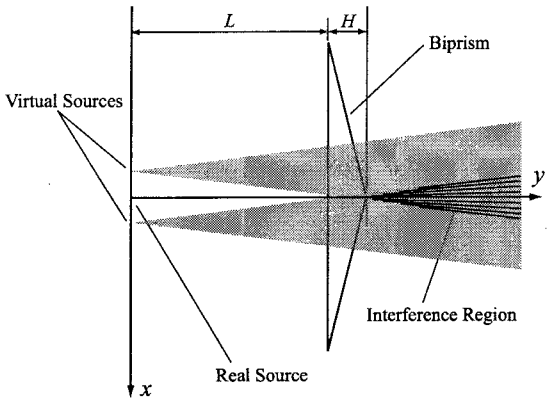

Figure 9: The equivalent virtual sources of the refracted lights of a biprism

decreasing the distance L and the thickness H so that the virtual sources approach to the wall.

The interference patterns created by smaller L and H are depicted in Fig. 10 and Fig. 11. The values used for the calculation is the same as the previous section except for setting L=1 mm and H=0.5 mm. The offsets of the fringe spacings of both types of configurations are reduced and the fringe patterns approach to fan-like shapes. The offsets of the fringe spacings can be reduced if the micro fabrication of optics is available.

CONCLUDING REMARKS

An optical method for the measurement of local wall shear stress was proposed. The method utilizes a Fresnel's biprism to create light interference pattern near the wall. It was aimed for the application to high Reynolds number flows where a sensor of slit type configuration can not be applied.

We proposed two types configurations of sensors in this paper and investigated the principle and the measurement volume. The interference patterns created by the configurations are calculated by electromagnetic theory. The interference pattern were created just above from the wall as expected. However the resulting interference pattern were not suitable for the local wall shear stress measurement because of the offsets of fringe spacings at the wall surface. The offsets can be reduced by decreasing the incidence distance

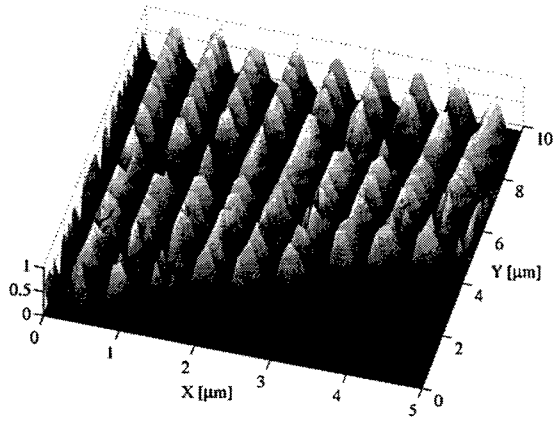

Figure 10: The interference pattern created by the type I sensor with smaller L and H with respect to the Fig.5 (L=1 mm, H=0.5 mm)

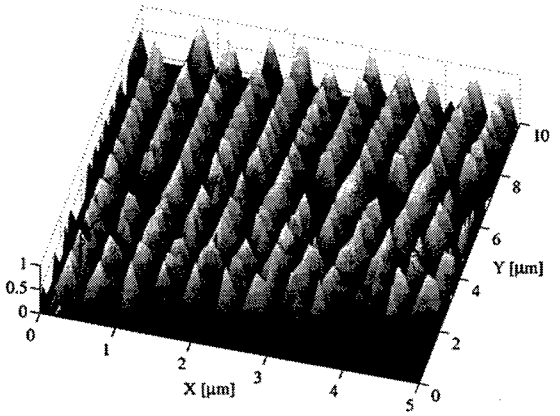

Figure 11: The interference pattern created by the type II sensor with smaller L and H with respect to the Fig.6 (L=1 mm, H=0.5 mm)

from the light source to the biprism and the thickness of the biprism. Considerations are required before the method is applied to the measurement in a flow.

REFERENCES

Albrecht, H. E., Borys, M., Damaschke, N., and Tropea, C., 2002, "Laser Doppler and Phase Doppler Measurement Techniques", Springer.

Alfredsson, H. P., Johansson, V. A., Haritonidis, H. J., and Eckelmann, H., 1988, "The fluctuating wall-shear stress and the velocity field in the viscous sublayer", *Phys. Fluids*, Vol. 31, pp. 1026-1033.

Born, M., and Wolf, E., 1999, "Principles of Optics (7th (expanded) ed.)", Cambridge University Press.

Chandrasekaran, V., Cain, A. Nishida, T., Cattafesta, L. N., and Sheplak, M., 2001, "Characterization of a Micromachined Thermal Shear Stress Sensor", *39th Aerospace Sciences Meeting and Exhibit*, Reno, AIAA Paper 2001-0247.

Czarske, J., Büttner, L., Razik, T., and Müller, H., 2002, "Boundary layer velocity measurements by a laser Doppler profile sensor with micrometre spatial resolution", *Mes. Sci. Technol.*, Vol. 13, pp. 1979-1989.

Durst, F., Jovanović, J., and Sender, J., 1995, "LDA measurements in the near-wall region of a turbulent pipe flow", *J. Fluid Mech.* Vol. 295, pp. 305-335.

Durst, F., Fischer, M., Jovanović, J., and Kikura, H., 1998, "Methods to set up and investigate low Reynolds number, fully developed plane channel flow", *Trans. ASME J. Fluid Eng.*, Vol. 120, pp. 496-503.

Haritonidis, J. H., 1989, "The measurement of wall shear stress", *Advances in Fluid Mechanics Measurements*, Lecture Notes in Engineering Vol. 45, ed., Brebbia, C. A., Orszag, S. A., and Gad-el-Hak, M., Springer, pp. 229-261.

Hecht, E., 2002, "Optics (4th ed.)", Addison Wesley.

Löfdahl, L., and Gad-el-Hak, M., 1999, "MEMS-based pressure and shear stress sensors for turbulent flows", *Mes. Sci. Technol.* Vol. 10, pp. 665-686.

Millerd, J. E., Swienton, J. P., Unterscher, F., Trolinger, J. D., Smith, L. G., and LaRue, J. C., 1996, "Holographic sensor for measurement of wall velocity gradients", *Exp. Fluids*, Vol. 21, pp. 469-476.

Naqwi, A. A., and Reynolds, W. C., 1984, "Dual cylindrical wave laser-Doppler method for measurement of wall shear stress" *Laser Anemometry in Fluid Mechanics -II*, ed Adrian, R. J., Durão, D. F. G., Durst, F., Mishima, H. and Whitelaw, J. H., LADOAN-Instituto Superior Técnico, Lisbon, pp. 105-122.

Naqwi, A. A., and Reynolds, W. C., 1991, "Measuring of turbulent wall velocity gradients using cylindrical waves of laser light" *Exp. Fluids*, Vol. 10, pp. 257-266.

Obi S., Inoue K., Furukawa T., and Masuda S., 1996, "Experimental study on the statistics of wall shear stress in turbulent channel flows", *Int. J. Heat and Fluid Flow*, Vol. 17, pp. 187-192.

Padmanabhan, A., Goldberg, H., Breuer, K. D., and Schmidt, M. A., 1996, "A wafer-bounded floating-element shear stress microsensor with optical position sensing by photodioides", *J. Microelectromechanical Systems*, Vol. 5, pp. 307-15.

Sumita Optical Glass Inc., 2002, "Optical Glass Data Book", http://www.sumita-opt.co.jp

Sun H. J., 1987, "Frequency modulation instruments for skin friction", *12th International Congress on Instrumentation in Aerospace Simulation Facilities*, Williamsburg, IEEE. Cat. No.87CH2449-7, pp. 378-385.

Sun H. J., and Qe J. Y., 1991, "Application of biprism shear strainratemeter in two dimensional channel flow", *14th International Congress on Instrumentation in Aerospace Simulation Facilities* Rockville, IEEE. Cat. No. 91CH3028-8, pp. 240-245.